JACS
JOURNAL OF THE AMERICAN CHEMICAL SOCIETY
pubs.acs.org/JACS
Communication

Barrier-Lowering Effects of Baird Antiaromaticity in Photoinduced Proton-Coupled Electron Transfer (PCET) Reactions

Lucas J. Karas,* Chia-Hua Wu, and Judy I. Wu*

Cite This: J. Am. Chem. Soc. 2021, 143, 17970−17974
Read Online
ACCESS | Metrics & More | Article Recommendations | Supporting Information

ABSTRACT: Many popular organic chromophores that catalyze photoinduced proton-coupled electron transfer (PCET) reactions are aromatic in the ground state but become excited-state antiaromatic in the lowest $\pi\pi^*$ state. We show that excited-state antiaromaticity makes electron transfer easier. Two representative photoinduced electron transfer processes are investigated: (1) the photolysis of phenol and (2) solar water splitting of a pyridine−water complex. In the selected reactions, the directions of electron transfer are opposite, but the net result is proton transfer following the direction of electron transfer. Nucleus-independent chemical shifts (NICS), ionization energies, electron affinities, and PCET energy profiles of selected $[4n]$ and $[4n + 2]$ π-systems are presented, and important mechanistic implications are discussed.

Photoinduced proton-coupled electron transfer (PCET) reactions are the critical steps to a myriad of energy conversion processes in organic and bio-organic photochemistry.[1,2] In the case where an electron moves first, these reactions also can be called electron-driven proton transfer—an aromatic chromophore absorbs light, triggering the migration of an electron, and a proton follows. These reactions typically have low barriers, and here, we explain the origin of such low barriers, making the connection between facile electron transfer and the concepts of ground- and excited-state (anti)aromaticity. We note that the most common organic chromophores (e.g., phenol,[3] pyridine,[4] and indoles[5,6]) are Hückel $[4n + 2]$ aromatic in the ground state,[7] but become Baird $[4n + 2]$ antiaromatic in the lowest $\pi\pi^*$ state.[8] Excited-state antiaromaticity makes charge separation easier, and this relationship has important mechanistic consequences for the photochemical reactions of aromatic compounds.

A representative example is the photolytic O−H bond fission of phenol. Flash photolysis and transient absorption studies of phenol in the vapor phase and in aqueous solution indicate the formation of neutral phenoxy radicals.[9,10] Because photolysis produces $H^\bullet$ and $PhO^\bullet$, it is tempting for the trained organic chemist to illustrate bond dissociation by two sets of single-headed arrows showing homolytic cleavage of the OH σ-bond (Figure 1a, top). But the reaction cannot happen this way. The >95 kcal/mol homolytic O−H bond dissociation energy is much too high. According to *ab initio* studies and kinetic experiments, UV irradiation first generates an optically active $\pi\pi^*$ state, then O−H σ-bond fission resolves in a dark $\pi\sigma^*$ state, reached by nonadiabatic interaction of the two surfaces.[5,11−13] Photolytic O−H and N−H bond fission processes for other aromatic chromophores proceed through similar dissociative charge transfer.[3,6,14] Crossing of the $\pi\pi^*$ and $\pi\sigma^*$ states implies an alternative mechanism for OH photolysis that has never been recognized explicitly. We suggest that photolysis of phenol occurs through *heterolytic* cleavage of the polar O−H bond. Upon photoexcitation, an electron is transferred from the π-ring to H, and the polar O−H bond breaks heterolytically (Figure 1a, bottom).

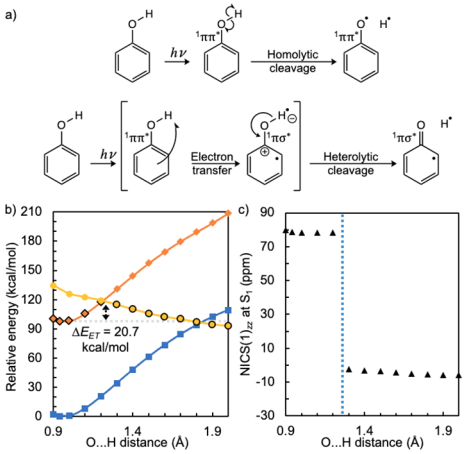

Figure 1. (a) Two different mechanistic representations for the photolysis of phenol. (b) Potential energy profiles along the O−H stretching coordinate, in the S_0 (blue squares), $^1\pi\pi^*$ (orange rhomboids), and $^1\pi\sigma^*$(yellow circles) states of phenol, and (c) $NICS(1)_{zz}$ values computed along the photoinduced PCET pathway (see markers with black border in 1b).

Figure 1b shows the potential energy profiles of the S_0, $^1\pi\pi^*$ (locally excited, LE), and $^1\pi\sigma^*$ (charge transfer, CT) states of phenol along the O−H stretching coordinate (at the S_0- and LE-state minima, and at points between O−H = 0.9 to 2.0 Å, at 0.1 Å intervals), computed at CASPT//CASSCF/6-

Received: September 2, 2021
Published: October 21, 2021

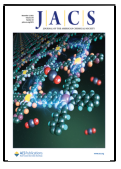

https://doi.org/10.1021/jacs.1c09324
J. Am. Chem. Soc. 2021, 143, 17970−17974

311+G(d,p) (see full methods in the Supporting Information, SI). Homolytic cleavage of the O−H bond requires >95 kcal/mol in both the S_0 and the $^1\pi\pi^*$ states; see parallel displaced S_0 and $^1\pi\pi^*$ curves in Figure 1b. Heterolytic cleavage of the polar O−H bond requires much less energy and occurs readily upon crossing of the $^1\pi\pi^*$ and $^1\pi\sigma^*$ states. Estimated barriers to electron transfer (ΔE_{ET}) were derived by the energy at the crossing of the interpolated $\pi\pi^*$ and $\pi\sigma^*$ curves minus the energy of the $\pi\pi^*$-state minimum. Note that the intersecting point of the yellow and orange curves in Figure 1 is not a minimal energy crossing point (MECP) on the potential energy surface, since the geometries for each state were optimized separately. Past the conical intersection, an electron transfers from the photoexcited [4*n* + 2] π-ring ("anti-aromatic") to the phenolic H through a low estimated barrier ($\Delta E_{ET} \approx 20$ kcal/mol, at O−H = 1.21 Å), and the $^1\pi\sigma^*$ state is stabilized as the proton follows the electron, producing $H^\bullet$ and $PhO^\bullet$. A heterolytic bond O−H bond dissociation pathway is further supported by charge analysis data included in Figure S9. We note that closely related reactions such as the photo-Fries rearrangement of phenyl esters also are commonly illustrated in Google searches and textbooks as homolytic O−R bond cleavage processes. We suggest that the arrow pushing mechanisms of these reactions also ought to be redrawn.[15,16]

But why should the barrier to electron transfer be so low? Note in Figure 1b, that a low ΔE_{ET} barrier is in part due to a high $^1\pi\pi^*$-state energy. This may be explained by Baird antiaromaticity of the [4*n* + 2] π-ring. Phenol is Hückel [4*n* + 2] aromatic in the S_0 state but becomes Baird [4*n* + 2] antiaromatic in the lowest $^1\pi\pi^*$ state,[17−20] and reversal of the Hückel rule drives electron transfer. Computed nucleus-independent chemical shifts, $NICS(1)_{zz}$, at geometries along the photoinduced PCET pathway (Figure 1c) confirm that phenol is antiaromatic in the $^1\pi\pi^*$ state (large positive $NICS(1)_{zz}$ values) and show that paratropicity of the π-ring drops immediately past the $^1\pi\pi^*$- and $^1\pi\sigma^*$-state intersection (see also Figure S5 for T_1-state results). $NICS(1)_{zz}$ data were computed at 1 Å above the ring centers including only the out-of-plane (*zz*) shielding tensor with an inverted sign.[21−23] $NICS(1)_{zz}$ data were computed at CASSCF/6-311+G(d,p) for **1**, **1′**, phenol, and the (Py)−water complex and at CASSCF/6-31G(d,p) for **2** and **2′**. Negative $NICS(1)_{zz}$ values indicate aromaticity, and positive $NICS(1)_{zz}$ values indicate antiaromaticity.

Of course, photoexcitation promotes the energy of any molecule, increasing both the ability to donate and to accept an electron. But this effect is especially pronounced for compounds with antiaromatic character in the lowest $\pi\pi^*$ states. We show this connection in Figure 2, by comparing the computed ionization energies (IE) and electron affinities (EA) of a set of [4*n* + 2] and [4*n*] annulenes to their nonaromatic isomers, in the S_0 and T_1 states.[24] Zhu and Schleyer have shown that the isomerization energies of the T_1 states of such pairs provide reliable energetic measures for triplet state (anti)aromaticity[25] Toluene is Hückel [4*n* + 2] aromatic in the S_0 state but Baird antiaromatic in the T_1 state and shows significantly reduced IE (ΔIE = 203.0−122.9 = 80.1 kcal/mol) and EA (ΔEA = 48.6 + 45.9 = 94.5 kcal/mol) values in the excited state (Figure 2a, left), compared to those of the nonaromatic methylenecyclohexadiene (ΔIE = 36.9 kcal/mol, ΔEA = 39.5 kcal/mol) (Figure 2a, right). Figure 2b shows the opposite example. Planar methyl-cyclooctatetraene (COT) is Hückel [4*n*] antiaromatic in the S_0 state but Baird aromatic in the T_1 state and exhibits only modestly lowered IE (ΔIE = 8.0 kcal/mol) and EA (ΔEA = 8.5 kcal/mol) values in the excited state (Figure 2b, left), compared to those of the nonaromatic isomer (ΔIE = 36.1 kcal/mol, ΔEA = 36.3 kcal/mol, Figure 2b, right). A significant drop in IE and EA values, because of excited-state antiaromaticity, makes charge transfer easier.

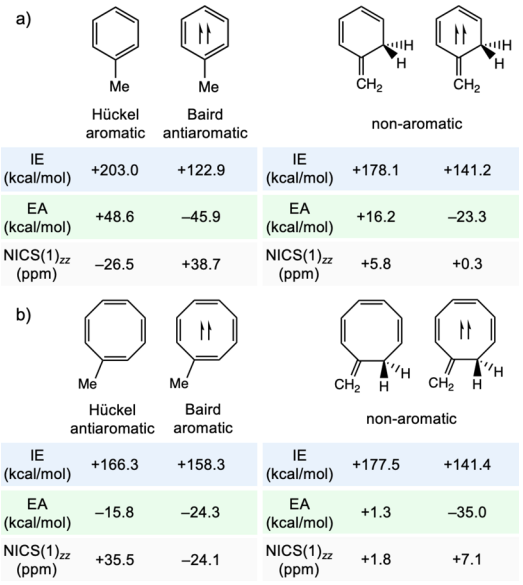

Figure 2. Computed ionization energies (IE), electron affinities (EA), and $NICS(1)_{zz}$ values for (a) toluene vs methylenecyclohexadiene and (b) planar methyl-COT vs planar methylenecyclooctatriene.

Figure 3 compares the T_1-state PCET profiles of 4-methylphenol (**1**, [4*n* + 2]) and 1-hydroxy-5-methyl-COT (**2**, [4*n*]) with those of their nonaromatic isomers (**1′** and **2′**). Potential energy profiles along the O−H stretching coordinate were computed at 0.1 Å intervals in the $^3\pi\pi^*$ and $^3\pi\sigma^*$ states (see Figure S4 for the S_1-state results). As the O−H bond stretches, the $^3\pi\pi^*$ and $^3\pi\sigma^*$ curves intersect, and crossing of the two functions marks the point at which an electron transfers from the π-ring to the phenolic H. **1** (Baird antiaromatic) displays a high T_1-state energy (80.7 kcal/mol), and the $^3\pi\pi^*$ to $^3\pi\sigma^*$ intersection occurs "early" through a relatively low barrier ($\Delta E_{ET} \approx 27$ kcal/mol, crossing at O−H = 1.26 Å) (Figure 3a, left). In contrast, **1′** (nonaromatic) exhibits a lower T_1-state energy (38.3 kcal/mol), and the conical intersection occurs "late" through a nearly doubled barrier ($\Delta E_{ET} \approx 57$ kcal/mol, crossing at O−H = 1.47 Å) (Figure 3b, left). Computed $NICS(1)_{zz}$ values for **1**, at geometries along the photoinduced PCET pathway, show an abrupt drop in paratropicity past the $^3\pi\pi^*$ to $^3\pi\sigma^*$ intersection (Figure 3a, right, note the sign change of $NICS(1)_{zz}$ values from positive to negative), while those of **1′** remain constant for both the $^3\pi\pi^*$ and $^3\pi\sigma^*$ states, having values close to zero (Figure 3b, right). The high T_1-state energy of **1** is a result of Baird antiaromaticity, and facile electron transfer is the escape from it.

Potential energy profiles for the T_1 states of **2** vs **2′** show the opposite. **2** (Baird aromatic) exhibits a low T_1-state energy (5.9 kcal/mol), and crossing from the $^3\pi\pi^*$ state to the $^3\pi\sigma^*$ state involves a high barrier ($\Delta E_{ET} \approx 70$ kcal/mol, at O−H = 1.56 Å) due to a largely stabilized T_1 state (Figure 3c, left). In comparison, **2′** (nonaromatic) has a higher T_1-state energy (31.5 kcal/mol) and a lower barrier to electron transfer ($\Delta E_{ET} \approx 56$ kcal/mol, at O−H = 1.47 Å) (Figure 3d, left, note the

https://doi.org/10.1021/jacs.1c09324
J. Am. Chem. Soc. 2021, 143, 17970−17974

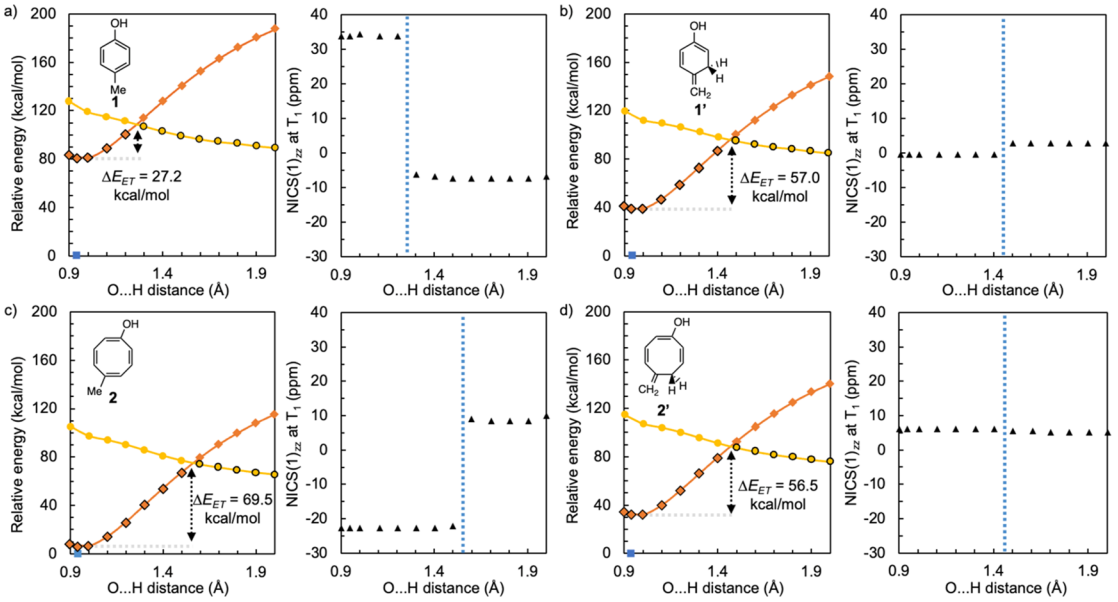

Figure 3. Potential energy profiles along the O−H stretching coordinate in the $^3\pi\pi^*$ (orange rhomboids) and $^3\pi\sigma^*$ (yellow circles) states for (a) **1**, (b) **1′**, (c) **2**, and (d) **2′**. NICS(1)$_{zz}$ values were computed along the photoinduced PCET pathway as indicated by points with a black marker border on the potential energy curve; the vertical blue dotted lines indicate crossing of the $^3\pi\pi^*$ and $^3\pi\sigma^*$ states.

similar T_1 energies and ΔE_{ET} values compared to **1′**, cf. Figure 2b). Computed NICS(1)$_{zz}$ values at geometries along the photoinduced PCET pathway of **2** increases in paratropicity past the $^3\pi\pi^*$ to $^3\pi\sigma^*$ intersection (Figure 3c, right, note sign change of NICS(1)$_{zz}$ values), while those of **2′** remain relatively constant for both the $^3\pi\pi^*$ and $^3\pi\sigma^*$ states (Figure 3d, right). Computed gauge-including magnetically induced current (GIMIC)[26] plots, ^{1}H chemical shifts, and the harmonic oscillator model of aromaticity (rHOMA)[27] agree with NICS; see the data in the SI.

We further considered the phototriggered water-splitting reaction of a model pyridine (Py)−water complex. In this example, an electron transfers from water to the aromatic core. Photodeactivation through PCET was suggested as a reason for the absence of fluorescence of pyridine in water.[4,28−31] Water splitting through this route requires two photons. In the first step, pyridine absorbs light ($\pi\pi^*$, LE state), and an electron moves from water to the photoexcited π-ring followed by proton transfer ($\pi\pi^*$ or nπ^*, CT state), generating a PyH$^\bullet$ and OH$^\bullet$ radical pair. The triplet CT state is degenerate with the singlet state and can be reached through efficient intersystem crossing. Photoreactions on the excited singlet and triplet state surfaces were shown to be quite similar. In the next step, a second photon detaches H$^\bullet$ from PyH$^\bullet$ and regenerates the catalytic pyridine. Without the chromophore, homolytic bond cleavage of the water O−H bond (in the gas phase) is is 5.1 eV (117.6 kcal/mol).[32] Here, we examine the first step of the reaction, showing that in the lowest $\pi\pi^*$ state the catalytic pyridine ring is Baird antiaromatic and that moving an electron from water to the pyridine ring alleviates excited-state antiaromaticity.

Figure 4b shows the computed energy profiles of the (Py)−water complex at 0.1 Å intervals along the N−H bond forming coordinate (i.e., H moving from water to the pyridinyl N) in the S_0 state, LE state ($^1\pi\pi^*$), and CT state (^{1}nπ^*, i.e., electron transfer from the hybridized lone pair of O). It was shown that crossing from the $^1\pi\pi^*$ LE state to the $^1\pi\pi^*$ CT state (i.e., electron transfer from the unhybridized lone pair of O)

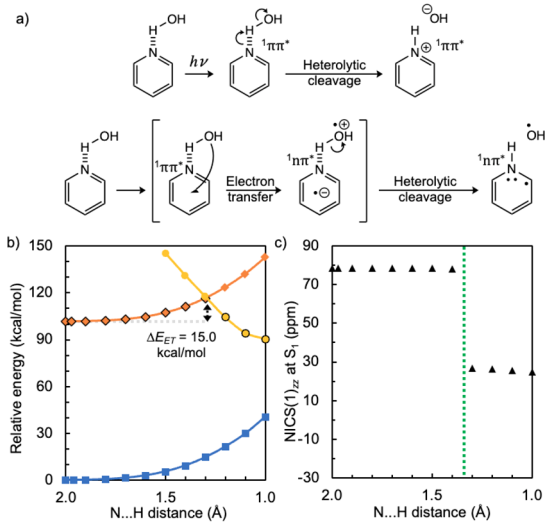

Figure 4. (a) Two different mechanistic representations for O−H bond breaking in the water-splitting reaction of (Py)−water. (b) Potential energy profiles along the N−H bond forming coordinate, in the S_0 (blue squares), $^1\pi\pi^*$ (orange rhomboids), and ^{1}nπ^* (yellow circles) states for the (Py)−water complex, and (c) NICS(1)$_{zz}$ values computed along the photoinduced PCET pathway.

produced a similar energetic profile.[4] As the N−H bond forms, the $^1\pi\pi^*$ and ^{1}nπ^* curves intersect, and crossing of the two functions marks the point at which an electron transfers from water to the π-ring, first forming a zwitterionic complex, followed by proton transfer leading to the homolytic products PyH$^\bullet$ and OH$^\bullet$ (Figure 4a, bottom). Without electron transfer from water to the pyridinyl ring, the water O−H bond breaks heterolytically to give the products, PyH$^+$ and OH$^-$ (Figure 4a, top). Computed NICS(1)$_{zz}$ values at geometries along the reaction pathway show a drop in paratropicity past the LE- and CT-state intersection (Figure 4c, see Figure S6 for T_1 results). A heterolytic bond O−H bond dissociation pathway leading to

https://doi.org/10.1021/jacs.1c09324
J. Am. Chem. Soc. 2021, 143, 17970−17974

homolytic products is further supported by charge analyses data (Figure S10).

Traditionally, the driving force for photoinduced electron transfer has been explained by the Rehm−Weller model,[33] where Gibbs free energy for charge separation is estimated by oxidation/reduction potentials of the electron donor/acceptor. Here, we show that a more complete picture emerges when the effects of excited-state (anti)aromaticity[34−43] are considered. Even though all photoexcited molecules can be thought to be "unstable," Baird antiaromaticity is a useful effect for tuning the energy levels of $\pi\pi^*$ states and the many reactions that proceed through these bright states.

■ ASSOCIATED CONTENT

Supporting Information

The Supporting Information is available free of charge at https://pubs.acs.org/doi/10.1021/jacs.1c09324.

Details of the computational methods, optimized Cartesian coordinates, computed ^{1}H chemical shifts, rHOMA, GIMIC, charge analyses, as well as NICS(1)$_{zz}$ and PCET energy profiles of **1** and **1′** in the S_1 state, and phenol and (Py)−water in the T_1 state are included (PDF)

■ AUTHOR INFORMATION

Corresponding Authors

Judy I. Wu − *Department of Chemistry, University of Houston, Houston, Texas 77204, United States;* orcid.org/0000-0003-0590-5290; Email: jiwu@central.uh.edu

Lucas J. Karas − *Department of Chemistry, University of Houston, Houston, Texas 77204, United States;* orcid.org/0000-0001-7970-119X; Email: lucaskaras@gmail.com

Author

Chia-Hua Wu − *Department of Chemistry, University of Houston, Houston, Texas 77204, United States;* orcid.org/0000-0001-6850-3024

Complete contact information is available at: https://pubs.acs.org/10.1021/jacs.1c09324

Notes

The authors declare no competing financial interest.

■ ACKNOWLEDGMENTS

J.I.W. thanks the National Science Foundation (CHE-1751370), the National Institute of General Medical Sciences of the National Institute of Health (R35GM133548), and the Alfred P. Sloan Research Foundation (FG-2020-12811) for support. We acknowledge the use of the Sabine cluster and support from the Research Computing Data Core at the University of Houston. Particularly, we thank Professor Henrik Ottosson for helpful suggestions for improving the manuscript.

■ REFERENCES

(1) Weinberg, D. R.; Gagliardi, C. J.; Hull, J. F.; Murphy, C. F.; Kent, C. A.; Westlake, B. C.; Paul, A.; Ess, D. H.; McCafferty, D. G.; Meyer, T. J. Proton-coupled electron transfer. *Chem. Rev.* **2012**, *112*, 4016−4093.

(2) Gagliardi, C. J.; Westlake, B. C.; Kent, C. A.; Paul, J. J.; Papanikolas, J. M.; Meyer, T. J. Integrating proton coupled electron transfer (PCET) and excited states. *Coord. Chem. Rev.* **2010**, *254*, 2459−2471.

(3) Domcke, W.; Sobolewski, A. L. Unraveling the molecular mechanism of photoacidity. *Science* **2003**, *302*, 1693−1694.

(4) Liu, X.; Sobolewski, A. J.; Borrelli, R.; Domcke, W. Computational investigation of the photoinduced homolytic dissociation of water in the pyridine-water complex. *Phys. Chem. Chem. Phys.* **2013**, *15*, 5957−5966.

(5) Ashfold, M. N. R.; Cronin, B.; Devine, A. L.; Dixon, R. N.; Nix, M. G. D. The role of $\pi\sigma^*$ excited states in the photodissociation of heteroaromatic molecules. *Science* **2006**, *312*, 1637−1640.

(6) Sobolewski, A. L.; Domcke, W. Computational studies of the photophysics of hydrogen-bonded molecular systems. *J. Phys. Chem. A* **2007**, *111*, 11725−11735.

(7) Hückel, E. Z. Quantentheoretische beiträge zum benzolproblem. *Eur. Phys. J. A* **1931**, *70*, 204−286.

(8) Baird, N. C. Quantum organic photochemistry: II. Resonance and aromaticity in the lowest $^3\pi\pi^*$ state of cyclic hydrocarbons. *J. Am. Chem. Soc.* **1972**, *94*, 4941−4948.

(9) Land, E. J.; Porter, G. Primary photochemical processes in aromatic molecules. Part. 7.—spectra and kinetics of some phenoxyl derivatives. *Trans. Faraday Soc.* **1963**, *59*, 2016−2026.

(10) Dobson, G.; Grossweiner, L. I. Flash photolysis of aqueous phenol and cresols. *Trans. Faraday Soc.* **1965**, *61*, 708−714.

(11) Sobolewski, A. L.; Domcke, W. Photoinduced electron and proton transfer in phenol and its clusters with water and ammonia. *J. Phys. Chem. A* **2001**, *105*, 9275−9283.

(12) Sobolewski, A. L.; Domcke, W.; Dedonder-Lardeux, C.; Jouvet, C. Excited-state hydrogen detachment and hydrogen transfer driven by repulsive $^1\pi\sigma^*$ states: a new paradigm for nonradiative decay in aromatic biomolecules. *Phys. Chem. Chem. Phys.* **2002**, *4*, 1093−1100.

(13) Nix, M. G. D.; Devine, A. L.; Cronin, B.; Dixon, R. N.; Ashfold, M. N. R. High resolution photofragment translational spectroscopy studies of the near ultraviolet photolysis of phenol. *J. Chem. Phys.* **2006**, *125*, 133318.

(14) Ashfold, M. N. R.; King, G. A.; Murdock, D.; Nix, M. G. D.; Oliver, T. A. A.; Sage, A. G. $\pi\sigma^*$ excited states in molecular photochemistry. *Phys. Chem. Chem. Phys.* **2010**, *12*, 1218−1238.

(15) Turro, N. J.; Ramamurthy, V.; Scaiano, J. C. *Modern molecular photochemistry of organic molecules*; University Science Books: Sausalito, CA, 2010; p 1084.

(16) Fries rearrangement. http://en.wikipedia.org/wiki/Fries_rearrangement, accessed March 22, 2021.

(17) Aihara, J.-I. Aromaticity-based theory of pericyclic reactions. *Bull. Chem. Soc. Jpn.* **1978**, *51*, 1788−1792.

(18) Karadakov, P. B. Ground- and excited-state aromaticity and antiaromaticity in benzene and cyclobutadiene. *J. Phys. Chem. A* **2008**, *112*, 7303−7309.

(19) Karadakov, P. B. Aromaticity and antiaromaticity in the low-lying electronic states of cyclooctatetraene. *J. Phys. Chem. A* **2008**, *112*, 12707−12713.

(20) Karadakov, P. B.; Hearnshaw, P.; Horner, K. E. Magnetic shielding, aromaticity, and bonding in the low-lying electronic states of benzene and cyclobutadiene. *J. Org. Chem.* **2016**, *81*, 11346−11352.

(21) Corminboeuf, C.; Heine, T.; Seifert, G.; Schleyer, P. v. R.; Weber, J. Induced magnetic field in aromatic [n]-annulenes—interpretation of NICS tensor components. *Phys. Chem. Chem. Phys.* **2004**, *6*, 273−276.

(22) Chen, Z.; Wannere, C. S.; Corminboeuf, C.; Puchta, R.; Schleyer, P. v. R. Nucleus-independent chemical shifts (NICS) as an aromaticity criterion. *Chem. Rev.* **2005**, *105*, 3842−3888.

(23) Gogonea, V.; Schleyer, P. v. R.; Schreiner, P. R. Consequences of triplet aromaticity in $4n\pi$-electron annulenes: calculation of magnetic shieldings for open-shell species. *Angew. Chem., Int. Ed.* **1998**, *37*, 1945−1948.

(24) Dahlstrand, C.; Yamazaki, K.; Kilsa, K.; Ottosson, H. Substituent Effects on the Electron Affinities and Ionization Energies of Tria-, Penta-, and Heptafulvenes: A Computational Investigation. *J. Org. Chem.* **2010**, *75*, 8060−8068.

(25) Zhu, J.; An, K.; Schleyer, P. v. R. Evaluation of triplet aromaticity by the isomerization stabilization energy. *Org. Lett.* **2013**, *15*, 2442−2445.
(26) Fliegl, H.; Taubert, S.; Lehtonen, O.; Sundholm, D. The gauge including magnetically induced current method. *Phys. Chem. Chem. Phys.* **2011**, *13*, 20500−20518.
(27) Krygowski, T. M. Crystallographic studies of inter- and intramolecular interactions reflected in aromatic character of π-electron systems. *J. Chem. Inf. Comput. Sci.* **1993**, *33*, 70−78.
(28) Reimers, J. R.; Cai, Z.-L. Hydrogen bonding and reactivity of water to azines in their S_1 (n,π*) electronic excited states in the gas phase and in solution. *Phys. Chem. Chem. Phys.* **2012**, *14*, 8791−8802.
(29) Liu, X.; Sobolewski, A. L.; Domcke, W. Photoinduced oxidation of water in the pyridine-water complex: comparison of the singlet and triplet photochemistries. *J. Phys. Chem. A* **2014**, *118*, 7788−7795.
(30) Esteves-López, N.; Coussan, S.; Dedonder-Lardeux, C.; Jouvet, C. Photoinduced water splitting in pyridine water clusters. *Phys. Chem. Chem. Phys.* **2016**, *18*, 25637−25644.
(31) Pang, X.; Jiang, C.; Xie, W.; Domcke, W. Photoinduced electron-driven proton transfer from water of an N-heterocylic chromophore: nonadiabatic dynamics studies for pyridine−water clusters. *Phys. Chem. Chem. Phys.* **2019**, *21*, 14073−14079.
(32) Maksyutenko, P.; Rizzo, T. R.; Boyarkin, O. V. A direct measurement of the dissociation energy of water. *J. Chem. Phys.* **2006**, *125*, 181101.
(33) Rehm, D.; Weller, A. Kinetics of fluorescence quenching by electron and H-atom transfer. *Isr. J. Chem.* **1970**, *8*, 259−271.
(34) Mohamed, R. K.; Mondal, S.; Jorner, K.; Delgado, T. F.; Lobodin, V. V.; Ottosson, H.; Alabugin, I. V. The missing C1−C5 cycloaromatization reaction: triplet state antiaromaticity relief and self-terminating photorelease of formaldehyde for synthesis of fulvenes from enynes. *J. Am. Chem. Soc.* **2015**, *137*, 15441−15450.
(35) Banerjee, A.; Halder, D.; Ganguly, G.; Paul, A. Deciphering the cryptic role of a catalytic electron in a photochemical bond dissociation using excited state aromaticity markers. *Phys. Chem. Chem. Phys.* **2016**, *18*, 25308−25314.
(36) Papadakis, R.; Li, H.; Bergman, J.; Lundstedt, A.; Jorner, K.; Ayub, R.; Haldar, S.; Jahn, B. O.; Denisova, A.; Zietz, B.; Lindh, R.; Sanyal, B.; Grennberg, H.; Leifer, K.; Ottosson, H. Metal-free photochemical silylations and transfer hydrogenations of benzenoid hydrocarbons and graphene. *Nat. Commun.* **2016**, *7*, 12962.
(37) Wu, C.-H.; Karas, L. J.; Ottosson, H.; Wu, J. I. Excited-state proton transfer relieves antiaromaticity in molecules. *Proc. Natl. Acad. Sci. U. S. A.* **2019**, *116*, 20303−20308.
(38) Lampkin, B. J.; Nguyen, Y. H.; Karadakov, P. B.; VanVeller, B. Demonstration of Baird's rule complementarity in the singlet state with implications for excited-state intramolecular proton transfer. *Phys. Chem. Chem. Phys.* **2019**, *21*, 11608−11614.
(39) Jorner, K.; Rabten, W.; Slanina, T.; Proos Vedin, N.; Sillen, S.; Wu Ludvigsson, J.; Ottosson, H.; Norrby, P.-O. Degradation of pharmaceuticals through sequential photon absorption and photoionization in amiloride derivatives. *Cell Rep. Phys. Sci.* **2020**, *1*, 100274.
(40) Halder, D.; Paul, A. Understanding the role of aromaticity and conformational changes in bond dissociation processes of photoprotecting groups. *J. Phys. Chem. A* **2020**, *124*, 3976−3983.
(41) Karas, L. J.; Wu, C.-H.; Ottosson, H.; Wu, J. I. Electron-driven proton transfer relieves excited-state antiaromaticity in photoexcited DNA base pairs. *Chem. Sci.* **2020**, *11*, 10071−10077.
(42) Slanina, T.; Ayub, R.; Toldo, J.; Sundell, J.; Rabten, W.; Nicaso, M.; Alabugin, I.; Galvan, I. F.; Gupta, A. K.; Lindh, R.; Orthaber, A.; Lewis, R. J.; Grönberg, G.; Bergman, J.; Ottosson, H. Impact of excited-state antiaromaticity relief in a fundamental benzene photoreaction leading to substituted bicyclo[3.1.0]hexenes. *J. Am. Chem. Soc.* **2020**, *142*, 10942−10954.
(43) Oruganti, B.; Pal Kalapos, P.; Bhargav, V.; London, G.; Durbeej, B. Photoinduced changes in aromaticity facilitate electrocyclization of dithienylbenzene switches. *J. Am. Chem. Soc.* **2020**, *142*, 13941−13953.

https://doi.org/10.1021/jacs.1c09324
J. Am. Chem. Soc. 2021, 143, 17970−17974